

*ARMY RESEARCH LABORATORY*



**The Effects of Net-Shape Machining on the Performance of  
Al 2024-T3 Subjected to Axial Tension-Tension  
Fatigue Loads**

by Cyril Williams

**ARL-TR-5277**

**August 2010**

## **NOTICES**

### **Disclaimers**

The findings in this report are not to be construed as an official Department of the Army position unless so designated by other authorized documents.

Citation of manufacturer's or trade names does not constitute an official endorsement or approval of the use thereof.

Destroy this report when it is no longer needed. Do not return it to the originator.

# **Army Research Laboratory**

Aberdeen Proving Ground, MD 21005-5066

---

---

**ARL-TR-5277**

**August 2010**

---

---

## **The Effects of Net-Shape Machining on the Performance of Al 2024-T3 Subjected to Axial Tension-Tension Fatigue Loads**

**Cyril Williams**

**Weapons and Materials Research Directorate, ARL**

<b>REPORT DOCUMENTATION PAGE</b>			<i>Form Approved</i> <b>OMB No. 0704-0188</b>		
Public reporting burden for this collection of information is estimated to average 1 hour per response, including the time for reviewing instructions, searching existing data sources, gathering and maintaining the data needed, and completing and reviewing the collection information. Send comments regarding this burden estimate or any other aspect of this collection of information, including suggestions for reducing the burden, to Department of Defense, Washington Headquarters Services, Directorate for Information Operations and Reports (0704-0188), 1215 Jefferson Davis Highway, Suite 1204, Arlington, VA 22202-4302. Respondents should be aware that notwithstanding any other provision of law, no person shall be subject to any penalty for failing to comply with a collection of information if it does not display a currently valid OMB control number. <b>PLEASE DO NOT RETURN YOUR FORM TO THE ABOVE ADDRESS.</b>					
<b>1. REPORT DATE (DD-MM-YYYY)</b> August 2010		<b>2. REPORT TYPE</b> Final		<b>3. DATES COVERED (From)</b> 9/1/2009–2/1/2010	
<b>4. TITLE AND SUBTITLE</b> The Effects of Net-Shape Machining on the Performance of Al 2024-T3 Subjected to Axial Tension-Tension Fatigue Loads			<b>5a. CONTRACT NUMBER</b>		
			<b>5b. GRANT NUMBER</b>		
			<b>5c. PROGRAM ELEMENT NUMBER</b>		
<b>6. AUTHOR(S)</b> Cyril Williams			<b>5d. PROJECT NUMBER</b> AH80		
			<b>5e. TASK NUMBER</b>		
			<b>5f. WORK UNIT NUMBER</b>		
<b>7. PERFORMING ORGANIZATION NAME(S) AND ADDRESS(ES)</b> U.S. Army Research Laboratory ATTN: RDRL-WMP-B Aberdeen Proving Ground, MD 21005-5066			<b>8. PERFORMING ORGANIZATION REPORT NUMBER</b> ARL-TR-5277		
<b>9. SPONSORING/MONITORING AGENCY NAME(S) AND ADDRESS(ES)</b>			<b>10. SPONSOR/MONITOR'S ACRONYM(S)</b>		
			<b>11. SPONSOR/MONITOR'S REPORT NUMBER(S)</b>		
<b>12. DISTRIBUTION/AVAILABILITY STATEMENT</b> Approved for public release; distribution is unlimited.					
<b>13. SUPPLEMENTARY NOTES</b>					
<b>14. ABSTRACT</b> Surface texture and process defects resulting from net-shape machining of engineering materials are often ignored in the design analysis of machined components parts. In this investigation, the effects of net-shape machining on the fatigue life of 2024-T6 aluminum were studied. Specimens were prepared using Abrasive Water Jet (AWJ) machining and the surface texture resulting from machining was characterized using contact profilometry. Based on the results from the surface texture evaluation and axial tension-tension fatigue tests performed, it was found that the fatigue life of 2024-T6 aluminum is surface texture dependent. As the roughness increases, the fatigue strength of the 2024-T6 aluminum decreases. It was found that the notch depth of the machined surface plays an important role in both low and high cycle fatigue. However, the mechanisms involved at low cycle fatigue are not well understood.					
<b>15. SUBJECT TERMS</b> axial, tension, fatigue, net-shape, machining, roughness, notch effects					
<b>16. SECURITY CLASSIFICATION OF:</b>			<b>17. LIMITATION OF ABSTRACT</b>  UU	<b>18. NUMBER OF PAGES</b>  26	<b>19a. NAME OF RESPONSIBLE PERSON</b> Cyril Williams
<b>a. REPORT</b> Unclassified	<b>b. ABSTRACT</b> Unclassified	<b>c. THIS PAGE</b> Unclassified			<b>19b. TELEPHONE NUMBER (Include area code)</b> 410-278-8753

---

## Contents

---

<b>List of Figures</b>	<b>iv</b>
<b>List of Tables</b>	<b>v</b>
<b>1. Introduction</b>	<b>1</b>
<b>2. Background and Literature Survey</b>	<b>1</b>
<b>3. Methods and Materials</b>	<b>4</b>
<b>4. Results</b>	<b>7</b>
<b>5. Discussion</b>	<b>9</b>
<b>6. Conclusion</b>	<b>11</b>
<b>7. References</b>	<b>12</b>
<b>Distribution List</b>	<b>14</b>

---

## List of Figures

---

Figure 1. A plot of surface factor versus surface roughness (Shigley and Mitchell, 1983).....	2
Figure 2. Sawtooth and sinusoidal profile of a machined surface. ....	3
Figure 3. Tension-tension fatigue test fixture. ....	4
Figure 4. Tensile fatigue specimen mounted in the MTS 810-load frame. ....	4
Figure 5. Surface texture of AWJ machined metals (Arola, 1996). ....	5
Figure 6. Geometry and dimensions of Al 2024-T3 specimens. ....	5
Figure 7. Censored S-N plot for Al 2024-T3 aluminum with two different levels of surface quality. ....	9

---

## List of Tables

---

Table 1. Experimental surface quality level design matrix for Al 2024-T3. ....	6
Table 2. AWJ cutting parameters used to achieve the 2 $\mu\text{m}$ and 6 $\mu\text{m}$ average roughness. ....	6
Table 3. Experimental load level design matrix for fatigue testing of the Al 2024-T3. ....	6
Table 4. Surface roughness parameters and the profile valley radii for Al 2024-T3. ....	7
Table 5. Core surface roughness parameters for the Al 2024-T3. ....	7
Table 6. Calculated Weibull parameters for the Al 2024-T3 censored data. ....	8

INTENTIONALLY LEFT BLANK.

---

## 1. Introduction

---

Military equipment, such as tanks, attack helicopters, armored personnel carriers (APCs), etc., are often subjected to repeated or cyclic loads that can lead to the development of physical microscopic damage. With an increase in the number of load cycles, the microscopic damage can coalesce into a well-defined crack. Cyclic crack growth then continues until catastrophic failure. Fatigue failures can occur at cyclic stresses well below the material's yield or ultimate strength. Due to changes in surface integrity and the presence of stress concentrations resulting from net-shape machining, fatigue damage usually develops on the surface of a component; consequently, surface topography has been found to have an appreciable effect on fatigue strength (Hanley and Dolan, 1953). Love (1952) has shown that the fatigue strength of a component increases as the surface roughness decreases and is also higher when the direction of polishing is parallel to the direction of applied stress.

Fatigue failures of conventional metals have been studied for more than 170 years and they account for the majority of mechanical failures in machine components (Dieter, 1991). It has been reported that the economic costs of fracture and its prevention are quite large, and it is estimated that 80% of these costs can be attributed to fatigue loading (Dowling, 1998). Due to the fatigue of materials, the annual cost to the U.S. economy is about 3% of the gross national product (GNP) and the same can be expected for other industrial nations (Dowling, 1998). In order to eliminate the economic costs associated with fracture and its prevention, the fatigue failure mechanisms in engineering materials must be thoroughly understood.

---

## 2. Background and Literature Survey

---

The fatigue strength of metals has been studied by a number of investigators. Based on the extent of literature and diversity of topics, a full review of the work conducted in this area is far beyond the scope of this study. The following literature survey will focus on relevant work related to the initiation and propagation of damage, analytical treatments of surface topography and fatigue damage, and their effects on the strength of metals.

The mechanical performance of engineering components has been found to be dependent on the surface integrity resulting from net-shape manufacturing. Therefore, it is important to account for the effects of surface integrity when designing engineering components. The effects of surface integrity on metals resulting from conventional manufacturing processes have been discussed extensively in the literature (Zahavi and Torbilo, 1996; Field et al., 1970; Murakami and Endo, 1983, 1987; Fordham et al., 1997; Mitchell, 1977; Arola and Williams, 2002). The

total fatigue life of engineering materials is comprised of the “initiation” life and “propagation” life. During fatigue loading, cracks most commonly initiate from surface defects that arise from manufacturing flaws. Hence, surface defects and/or a large surface roughness decrease the initiation component of fatigue life. Surface roughness, material properties, and the residual stress of the component surface layer are all important considerations in fatigue design.

The fatigue strength of metals is often considered in terms of the endurance limit or magnitude of applied cyclic stress below which the component exhibits infinite life. Shigley and Mischke (1989) have described the effects of surface integrity and other considerations on the endurance limit of metallic component using the relationship:

$$S_e = k_a k_b k_c k_d k_e k_f S'_e \quad (1)$$

where  $S_e$  is the corrected endurance limit, and  $S'_e$  is the inherent endurance limit of the material under fully reversed cyclic loading. The endurance limit in equation 1 is modified by correction factors where  $k_a$  is the surface factor,  $k_b$  is the size factor,  $k_c$  is the reliability factor,  $k_d$  is the temperature factor,  $k_e$  is the modifying factor for stress concentration, and  $k_f$  is the miscellaneous effects factor. The surface factor  $k_a$  is often represented in terms of the average roughness ( $R_a$ ), peak-to-valley height roughness ( $R_y$ ), or 10-point roughness ( $R_z$ ) of the machined surface in question as shown in figure 1. These parameters are defined in terms of the profile height distribution ( $z$ ) recorded over an assessment or traverse length ( $L$ ) according to equations 2–4.

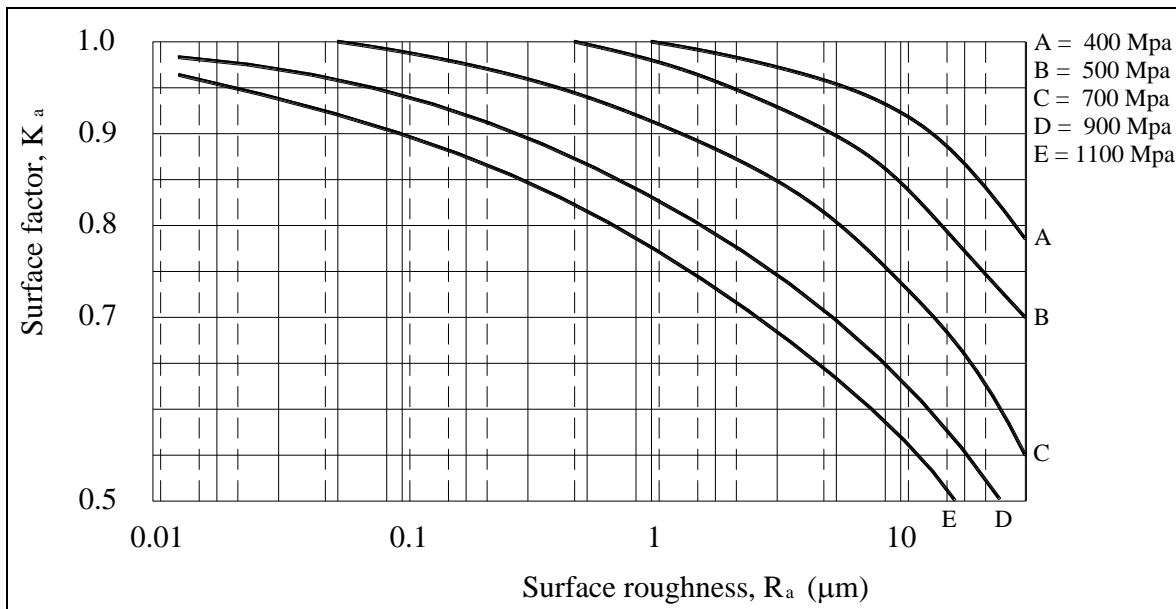


Figure 1. A plot of surface factor versus surface roughness (Shigley and Mitchell, 1983).

$$R_a = \frac{1}{L_0} \int |z| dx \quad (2)$$

$$R_y = |z_{\max} - z_{\min}| \quad (3)$$

$$R_z = \frac{1}{5} \left[ \sum_{i=1}^5 (z_i)_{\max} + \sum_{j=1}^5 (z_j)_{\min} \right] \quad (4)$$

Accordingly, the corrected endurance limit ( $S_e$ ) will decrease in a parabolic manner with increase in  $R_a$  (Shigley and Mitchell, 1983) according to equation 1. An increase in the ultimate strength of the component also reduces the endurance limit through  $k_a$  due to the changes in critical flaw size. Reductions in fatigue life through surface finish are attributed to the magnitude of surface stress concentration imposed by peak-to-valley height fluctuations. Furthermore, the notch root radius of the machined surface is also of interest as it dictates the shape of the notch. However, the quantity  $R_a$  does not provide a distribution sensitive description of a surface. For example, although the sawtooth and sinusoidal surface profiles for the machined surfaces shown in figure 2 have the same  $R_a$ ,  $R_y$ , and  $R_z$ ; however, the sawtooth profile would be much more detrimental to the fatigue life of a component by virtue of the notch root radius, i.e., as the notch root radius approaches infinity, the stress concentration factor tends to 1 or as the notch root radius approached zero, the stress concentration factor tends to infinity. Note that the surface factor for both surfaces in figure 2 would be the same according to figure 1 if based solely on  $R_a$ .

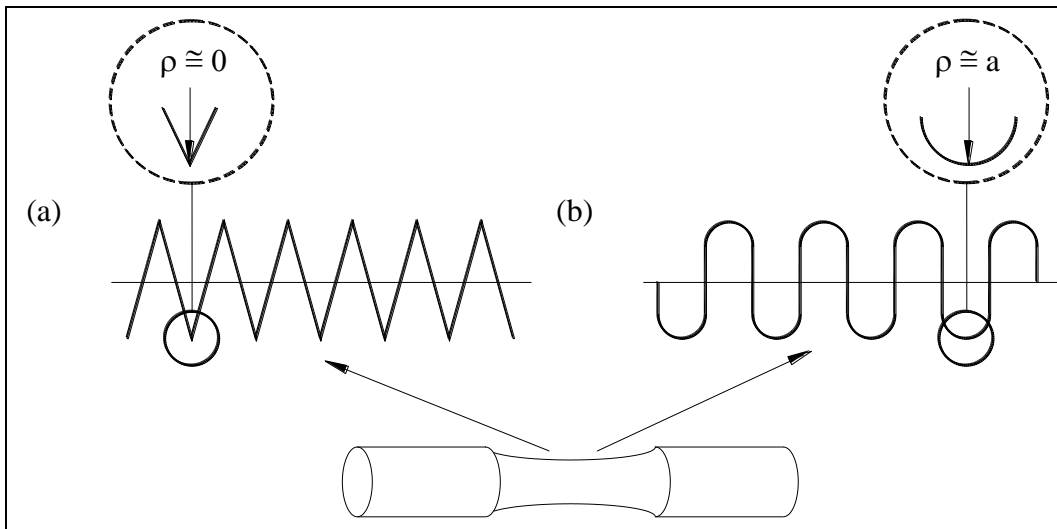


Figure 2. Sawtooth and sinusoidal profile of a machined surface.

It is therefore necessary to distinguish which surface roughness parameters provide an adequate distinction of the effects of surface topography on the fatigue strength of engineering materials. With this knowledge, an evaluation of the effects from machined surface topography on the fatigue strength of metals becomes more formidable.

---

### 3. Methods and Materials

---

Fatigue testing of engineering materials is generally conducted using rotating bending fatigue machines because they are reliable, cheap, and require little attention. However, rotating bending fatigue machines are not ideal for studying the fatigue characteristics of plate and sheet materials due to the complexity of developing stress concentrations at the edges. Because plate and sheet materials are widely used in military and aerospace applications, an alternative method of fatigue testing was necessary to fulfill the objectives of this study. An axial tension-tension fatigue test was conducted to determine the effects of surface texture resulting from Abrasive Water Jet (AWJ) machining on the fatigue strength of Al 2024-T3. The fatigue testing was conducted in accordance with ASTM E466-82 (ASTM, 1982) using the standard dogbone specimen geometry. To use existing equipment for the fatigue study, it was necessary to design and fabricate a test fixture for the chosen specimen geometry as shown in figure 3. The assembly was mounted within the grips of the MTS 810-tension/torsion load frame as shown in figure 4.

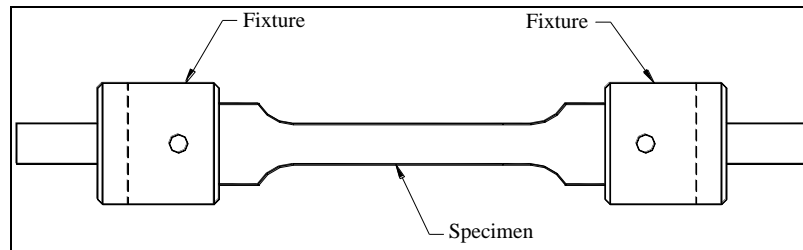


Figure 3. Tension-tension fatigue test fixture.



Figure 4. Tensile fatigue specimen mounted in the MTS 810-load frame.

Metallic materials machined using the AWJ exhibit three distinct macroscopic regions and they are comprised of the initial damage region (IDR), the smooth cutting region (SCR), and the rough cutting region (RCR) as shown in figure 5 (Arola, 1996). The only difference in microscopic features resulting from material removal in the SCR and RCR is the increase in abrasive particle deflection, whereas material in the IDR exhibits considerable deformation due to the nearly normal repeated impact of abrasives on the jet periphery. Hence, it was necessary to minimize the IDR in machining the fatigue specimens and extend the SCR over the entire thickness of the metal.

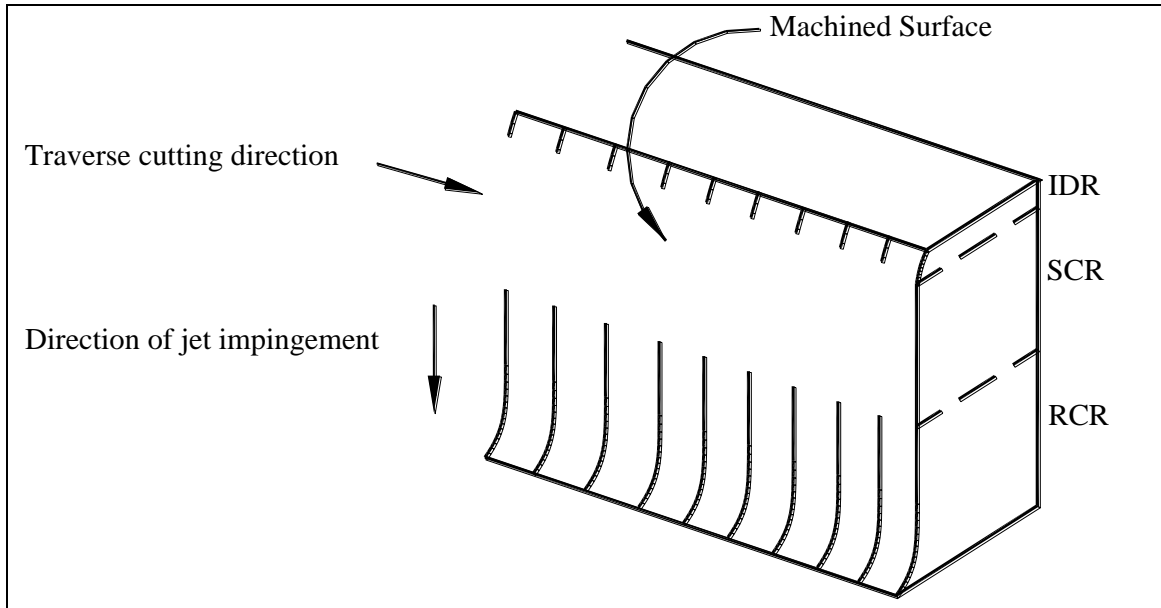


Figure 5. Surface texture of AWJ machined metals (Arola, 1996).

The Al 2024-T3 dogbone specimens were machined using an Omax Model 2652 abrasive waterjet unit. The dimensions for the metal specimens are shown in figure 6 and are in accordance with ASTM E466-82 (ASTM, 1982).

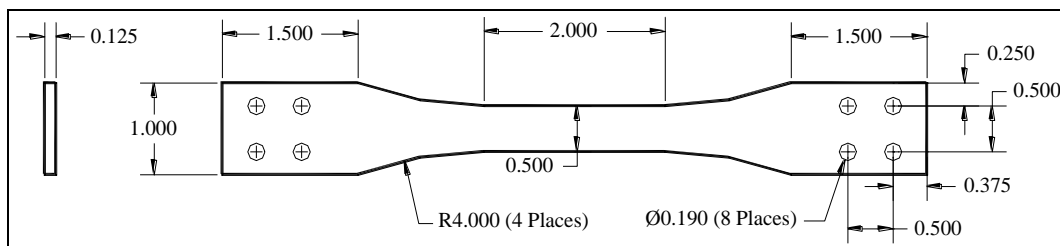


Figure 6. Geometry and dimensions of Al 2024-T3 specimens.

A design matrix for fatigue testing based on machined surface quality was developed for the Al 2024-T3 specimens as shown in table 1.

Table 1. Experimental surface quality level design matrix for Al 2024-T3.

Material	Quality Levels	
	Ra = 2 $\mu\text{m}$	Ra = 6 $\mu\text{m}$
Al2024-T3	56 specimens	56 specimens

A total of 112 aluminum specimens were machined using the AWJ machining center. As listed in table 1, two surface qualities with average roughness of 2  $\mu\text{m}$ , and 6  $\mu\text{m}$  were investigated. All 112 specimens were first edge trimmed using the AWJ to achieve a 6- $\mu\text{m}$  average roughness and then 56 were carefully polished using no. 220 and no. 400 grit sandpaper respectively in the AWJ traverse direction to achieve a 2- $\mu\text{m}$  average roughness. The cutting parameters used to obtain the 2- and 6- $\mu\text{m}$  average roughness are listed in table 2. The jewel and mixing tube diameter used for all AWJ machining were 0.31 mm and 0.76 mm, respectively. The machined surface topography of each Al 2024-T3 specimen was evaluated using contact profilometry to enable a quantification of the surface texture and apparent notch geometry resulting from the material removal process.

Table 2. AWJ cutting parameters used to achieve the 2- and 6- $\mu\text{m}$  average roughness.

Average Roughness	Pressure (Mpa)	Travel Speed (mm/s)	Standoff (mm)	Grit Size (Granet No.)	Abra. Flow Rate (g/s)
2 $\mu\text{m}$	310	7.63	0.8	80 <sup>a</sup>	0.8
6 $\mu\text{m}$	310	7.63	0.8	80	0.8

<sup>a</sup> Polished to final finish using no. 220 and no. 400 grit sandpaper.

The machined specimens were subjected to constant amplitude tension-tension axial fatigue loads. Eight specimens were tested at seven load levels that span the expected stress-life fatigue response; the fatigue load levels are listed in table 3.

Table 3. Experimental load level design matrix for fatigue testing of the Al 2024-T3.

Material	Stress Amplitude (MPa), R = 0.1						
	Level 1	Level 2	Level 3	Level 4	Level 5	Level 6	Level 7
Al2024-T3	83	93	124	140	175	198	206

All fatigue tests were conducted in load control at a frequency of 12 Hz and a stress ratio ( $R = \sigma_{\min} / \sigma_{\max}$ ) of 0.1. The load, displacement, and time were monitored during fatigue testing and recorded using Teststar II software, which is a commercially available data acquisition package for the MTS. Following failure of each specimen, the number of cycles to failure (N) was recorded and the fractured surface was inspected to determine the source of failure.

---

## 4. Results

---

The effects of net-shape machining on the fatigue strength of Al 2024-T3 was studied using tension-tension axial fatigue loading. AWJ machining was used to produce fatigue specimens and the roughness parameters, surface profile, and notch root radii for Al 2024-T3 resulting from the specified cutting conditions were measured and recorded. The effective notch root radius ( $\bar{\rho}$ ) was determined from the profile of each surface quality using the average radii of three prominent valleys as employed by Arola and Williams (2002) for other homogeneous metals. The effective notch root radii ( $\bar{\rho}$ ) determined for each level of surface quality are listed in table 4 with the conventional surface roughness parameters. Furthermore, the core roughness ( $R_K$ ), the reduced peak height ( $R_{PK}$ ), and valley depth ( $R_{VK}$ ) as defined according to DIN 4776 for each surface quality were calculated and listed in table 5. It is worth noting that all roughness measurements for the Al 2024-T3 were made parallel to the traverse cutting direction along the specimen gage section.

Table 4. Surface roughness parameters and the profile valley radii for Al 2024-T3.

Method	$R_a$ ( $\mu\text{m}$ )	$R_y$ ( $\mu\text{m}$ )	$R_z$ ( $\mu\text{m}$ )	$\bar{\rho}$ ( $\mu\text{m}$ )
AWJA	1.93	11.95	13.41	8.33
AWJB	6.09	32.71	32.99	7.29

Table 5. Core surface roughness parameters for the Al 2024-T3.

Method	$R_K$ ( $\mu\text{m}$ )	$R_{VK}$ ( $\mu\text{m}$ )	$R_{PK}$ ( $\mu\text{m}$ )
AWJA	5.23	5.81	1.70
AWJB	18.72	12.78	5.47

Weibull (1951) statistics were used to conduct a complete statistical analysis and description of the fatigue failure distribution of the AWJ machined specimens. A 2-parameter Weibull distribution (listed in equation 5) was used to determine the failure parameters for both surface qualities. The Weibull modulus or shape parameter ( $\beta$ ) and characteristic life or scale parameter ( $\alpha$ ) for each stress amplitude were determined from the experimental data and are listed in table 6. Furthermore,  $F(t)$  is the cumulative distribution function (CDF) and  $t$  is the time to failure.

$$F(t) = 1 - e^{-(t/\alpha)^\beta} \quad (5)$$

Table 6. Calculated Weibull parameters for the Al 2024-T3 censored data.

Stress Amplitude (MPa)	2 $\mu\text{m}$ (AWJA)		6 $\mu\text{m}$ (AWJC)	
	$\alpha$	$\beta$	$\alpha$	$\beta$
83	1227390	4	955892	3
93	487429	3	343967	19
124	85385	12	76450	9
140	60779	6	73325	5
175	14318	9	10485	10
198	6910	32	4506	11
206	5148	6	2904	5

From the Weibull parameters listed in table 6, the characteristic life or scale parameter ( $\alpha$ ) is consistently increasing with decrease in stress amplitude as expected, but the Weibull modulus or shape parameter ( $\beta$ ) show no apparent trend. Therefore, no conclusive information was obtained using Weibull statistics. However, a 95% confidence interval was used in conjunction with Weibull statistics to remove all outliers and develop a censored fatigue response for the Al 2024-T3 aluminum. The censored fatigue-life diagram for the two surface textures is shown in figure 7.

It is apparent from figure 7 that the fatigue strength of 2024-T3 aluminum increases with decreased surface roughness throughout the fatigue-life response. However, at low cycle fatigue (LCF) the increase was more prominent when compared to that at high cycle fatigue (HCF). In general, the fatigue strength of a notched specimen is lower than that of an unnotched specimen, especially at HCF and this is attributed to the stress concentration developed at the notch tip. The fatigue response within the HCF regime appears to be contradictory because the fatigue strength of the surface with 2- $\mu\text{m}$  average roughness even though higher, approaches that of the 6- $\mu\text{m}$  average roughness.

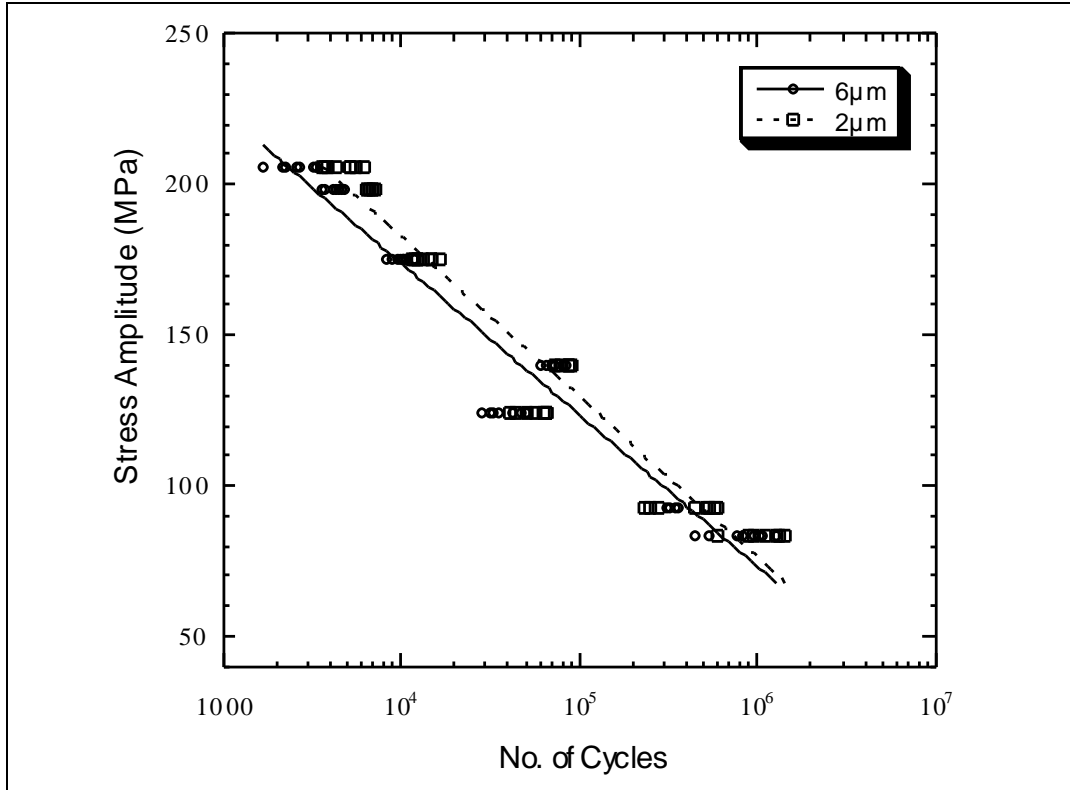


Figure 7. Censored S-N plot for Al 2024-T3 aluminum with two different levels of surface quality.

---

## 5. Discussion

---

The surface texture and surface integrity resulting from net-shape machining have been proven to be important considerations in mechanical design (Zahavi and Torbilo, 1996). The strength and/or service life of an engineering component is not only dependent on the material's intrinsic mechanical properties, but also on certain aspects of the machined surface such as surface texture.

In general, there is a gradual decrease in notch sensitivity with increasing alternating stress amplitude due to the increasing influence of plastic deformation (Frost and Dugdale, 1957). However, the contrast of the aforementioned statement is observed in the fatigue response diagram shown in figure 8. That is, there is an increase in notch sensitivity with increase in stress amplitude. Because the stresses are relatively low at HCF when compared to those at LCF and fatigue crack growth is usually the dominant failure mode. The Al 2024-T3 aluminum should become more sensitive to notches (i.e., increase in notch sensitivity) and therefore, the fatigue strength of the surface with 2- $\mu$ m average roughness should deviate from that of the

6- $\mu\text{m}$  average roughness. Because the AWJ cutting parameters for both surfaces are identical (see table 2), this implies that the difference in the notch root radii for both profiles would be identical and this can be observed in table 4. The characteristic difference between the two surface profiles is their notch depth. For the surface with the 2- $\mu\text{m}$  average roughness, the notch depth was observed to be less than that of the 6  $\mu\text{m}$  due to polishing. Because the elastic stress concentration is dependent not only on the notch root radius but also on the notch depth, the surface with the 6  $\mu\text{m}$  exhibited higher stress concentration and hence a lower fatigue strength. This is clearly evident when considering elastic stress concentration models such as the Peterson (1974), Arola-Ramulu (1998), and Neuber (1958) models. From the Peterson model listed in equation 6, it is apparent that the elastic stress concentration is dependent on both the notch depth and profile valley radius. For the same notch root radius, the elastic stress concentration will decrease with a reduction in notch depth. Similarly, for the Neuber and Arola-Ramulu models listed in equations 7 and 8, respectively, the elastic stress concentration decreases with decrease in the standard roughness parameters. A decrease in notch depth usually results in a decrease in standard roughness parameters because they are directly dependent on both peaks and valleys.

$$K_t = 1 + 2\sqrt{\frac{t}{\rho}} \quad (6)$$

where  $t$  is the notch depth and  $\rho$  is the profile valley notch root radius.

$$K_t = 1 + n\sqrt{\lambda \frac{R_z}{\rho}} \quad (7)$$

where  $n$  represent the stress state,  $\lambda$  is the spacing factor,  $R_z$  is the ten-point roughness and  $\rho$  is the notch root radius.

$$\bar{K}_t = 1 + n \left( \frac{R_a}{\bar{\rho}} \right) \left( \frac{R_y}{R_z} \right) \quad (8)$$

where  $n$  is an empirical constant,  $R_a$ ,  $R_y$ ,  $R_z$ , and  $\rho$  are the average roughness, peak to valley height, ten-point roughness and effective notch root radius respectively.

Although both surfaces have similar notch root radius, the surface with 2- $\mu\text{m}$  roughness exhibited superior fatigue strength because of its lower notch depth. The difference in the fatigue strength for both surfaces at LCF is large when compared to that at HCF. This behavior is not well understood and it is contrary to what is expected for homogeneous materials (Arola and Williams, 2002). Using AISI 4130 CR steel Arola and Williams, 2002 were able to show that during cyclic loading the material continues to deform plastically in every cycle if the stress at the notch is to remain reduced. Therefore, the plastic strains that are induced during the cyclic

process can cause the stress amplitude to be less than the actual stress ( $K_t\sigma$ ) due to stress concentration at the notch, where  $K_t$  is the elastic stress concentration and  $\sigma$  is the nominal stress. Consequently, the redistribution of near-notch stress causes the fatigue life to be longer than expected. This redistribution of near-notch stress typically occurs at high stress amplitudes (corresponding to short fatigue lives) and is sometimes referred to as reversed yielding.

---

## **6. Conclusion**

---

Based on the results from the surface texture evaluation and axial tension-tension fatigue tests performed with Al 2024-T3 it can be concluded that the axial tension-tension fatigue response of Al 2024-T3 is surface texture dependent. As the surface roughness of the machined surface increases, the fatigue strength of the Al 2024-T3 aluminum decreases. It was found that the notch depth of the surface texture plays an important role in both LCF and HCF. However, the mechanisms involved at LCF (plasticity dominated regime) are not well understood at this point and more research is required to resolve the unanswered questions.

---

## 7. References

---

- Arola, D. *The Influence of Net-Shape Machining on the Surface Integrity of Metals and Fiber Reinforced Plastics*, Ph.D. Dissertation: University of Washington, 1996.
- Arola, D.; Williams, C. L. Estimating the Fatigue Stress Concentration Factor of Machined Surfaces. *International Journal of Fatigue* **2002**, *24*, pp. 923–930.
- Arola, D.; Ramulu, M., Net-Shape Manufacturing and the Process-Dependent Failure of Fiber-Reinforced Plastics Under Static Loads, *Journal of Composites Technology and Research*, JCTRER, Vol. 20, October **1998b**, pp. 210–220.
- Standard practice for conducting constant amplitude axial fatigue tests of metallic materials, ASTM E466-82. American Society for Testing and Materials, Philadelphia, 1982.
- Dowling, N. E. *Mechanical Behavior of Materials: Engineering Methods for Deformation, Fracture, and Fatigue*, Prentice Hall, 1999.
- Field, M. *Machining of High Strength Steels with Emphasis on Surface Integrity*, Air Force Machinability Data Center, Metcut Research Assoc., 1970, pp. 1–229.
- Fordham, J. D.; Pilkington, R.; Tang, C. C. The Effect of Different Profiling Techniques on the Fatigue Performance of Metallic Membranes of AISI 301 and Inconel 718. *International Journal of Fatigue* **1997**, *19* (6) pp. 487–501.
- Hanley, B. C.; Dolan, T. J. Surface Finish. *ASME: Metals Engineering-Design*, 1953, p. 100.
- Juinall, R. C.; Marshek, K. M. *Fundamentals of Machine Component Design*, John Wiley and Sons, 1991.
- Love, R. J. The Influence of Surface Condition on the Fatigue Strength of Steel. *Symposium Properties of Metallic Surface*, Institute of Metals, 1952, p. 161.
- Mitchell, M. R. Review of the Mechanical Properties of Cast Steels With Emphasis on Fatigue Behavior and the Influence of Microdiscontinuities. *Journal of Engineering Materials and Technology* **October 1977**, pp. 329–343.

- Murakami, Y.; Endo, M. Effects of an Artificial Small Defect on Torsional Fatigue Strength of Steels. *Journal of Engineering Materials and Technology* **1987**, *109*, pp. 124–129.
- Murakami, Y.; Endo, M. Quantitative Evaluation of Fatigue Strength of Metals Containing Various Small Defects or Cracks. *Engineering Fracture Mechanics* **1983**, *17* (1), pp. 1–15.
- Neuber, H. Kerbspannungslehre. *Springer-Verlag* **1958**, pp. 159–163.
- Peterson, R. E. Stress Concentration Factors, John Wiley and Sons, 1974.
- Shigley, J. E.; Mischke, C. R. Mechanical Engineering Design. *McGraw-Hill*, *5th Edition*, 1989.
- Shigley, J. E.; Mischke, C. R. Mechanical Engineering Design. *McGraw-Hill*, *4th Edition*, 1983.
- Weibull, W. *Journal of Applied Mechanics* **1951**, *18*, pp. 293–297.
- Zahavi, E.; Torbilo, V. Fatigue Design: Life Expectancy of Machine Parts, 1st Edition, CRC Press, 1996, p. 193.

NO. OF  
COPIES ORGANIZATION

1 DEFENSE TECHNICAL  
(PDF INFORMATION CTR  
only) DTIC OCA  
8725 JOHN J KINGMAN RD  
STE 0944  
FORT BELVOIR VA 22060-6218

1 DIRECTOR  
US ARMY RESEARCH LAB  
IMNE ALC HRR  
2800 POWDER MILL RD  
ADELPHI MD 20783-1197

1 DIRECTOR  
US ARMY RESEARCH LAB  
RDRL CIM L  
2800 POWDER MILL RD  
ADELPHI MD 20783-1197

1 DIRECTOR  
US ARMY RESEARCH LAB  
RDRL CIM P  
2800 POWDER MILL RD  
ADELPHI MD 20783-1197

1 DIRECTOR  
US ARMY RESEARCH LAB  
RDRL D  
2800 POWDER MILL RD  
ADELPHI MD 20783-1197

ABERDEEN PROVING GROUND

1 DIR USARL  
RDRL CIM G (BLDG 4600)

<u>NO. OF COPIES</u>	<u>ORGANIZATION</u>
1 (CD only)	DPTY ASSIST SCT FOR R&T SARD TT ASA (ACT) J PARMENTOLA THE PENTAGON RM 3E479 WASHINGTON DC 20310-1714
1	PRIN DPTY FOR TCHNLGY HQ US ARMY MATCOM AMCDCGR R PRICE 9301 CHAPEK RD FT BELVOIR VA 22060-5527
3	AIR FORCE ARMAMENT LAB AFATL DLJW W COOK D BELK J FOSTER EGLIN AFB FL 32542
2	NSF S MCKNIGHT G PAULINO 4201 WILSON BLVD, STE 545 ARLINGTON VA 22230-0002
2	DARPA W COBLENZ 3701 N FAIRFAX DR ARLINGTON VA 22203-1714
1	DIRECTOR US ARMY ARDEC AMSRD AAR AEE W E BAKER BLDG 3022 PICATINNY ARSENAL NJ 07806-5000
2	US ARMY TARDEC AMSTRA TR R MS 263 K BISHNOI D TEMPLETON MS 263 WARREN MI 48397-5000
1	COMMANDER US ARMY RSRCH OFC RDRL ROE N B LAMATTINA PO BOX 12211 RESEARCH TRIANGLE PARK NC 27709-2211

<u>NO. OF COPIES</u>	<u>ORGANIZATION</u>
1	COMMANDER US ARMY RSRCH OFC RDRL ROI M J LAVERY PO BOX 12211 RESEARCH TRIANGLE PARK NC 27709-2211
1	COMMANDER US ARMY RSRCH OFC RDRL ROE M D STEPP PO BOX 12211 RESEARCH TRIANGLE PARK NC 27709-2211
5	NAVAL RESEARCH LAB E R FRANCHI CODE 7100 M H ORR CODE 7120 J A BUCARO CODE 7130 J S PERKINS CODE 7140 S A CHIN BING CODE 7180 4555 OVERLOOK AVE SW WASHINGTON DC 20375
1	DTRA M GILTRUD 8725 JOHN J KINGMAN RD FORT BELVOIR VA 22060
1	ERDC US ARMY CORPS OF ENGINEERS USACEGSL P PAPADOS 7701 TELEGRAPH RD ALEXANDRIA VA 22315
1	AFOSR NL 875 NORTH RANDOLPH ST SUITE 325 RM 3112 F FAHROO ARLINGTON VA 22203
5	SOUTHWEST RSRCH INST C ANDERSON K DANNEMANN T HOLMQUIST G JOHNSON J WALKER PO DRAWER 28510 SAN ANTONIO TX 78284

NO. OF  
COPIES ORGANIZATION

1	COMPUTATIONAL MECH CONSULTANTS J A ZUKAS PO BOX 11314 BALTIMORE MD 21239-0314	M ZOLTOSKI RDRL WML B I BATYREV B RICE N WEINGARTEN RDRL WML D
1	APPLIED RSCH ASSOCIATES D E GRADY 4300 SAN MATEO BLVD NE STE A220 ALBUQUERQUE NM 87110	P CONROY M NUSCA RDRL WML G M BERMAN W DRYSDALE RDRL WML H
1	INTERNATIONAL RSRCH ASSOC INC D L ORPHAL 4450 BLACK AVE PLEASANTON CA 94566	T FARRAND R SUMMERS M FERREN-COKER L MAGNESS B SORENSON E KENNEDY
3	ORNL ENVIRONMENTAL SCI DIV W DOLL T GAMEY L BEARD PO BOX 2008 OAK RIDGE TN 37831	T EHLERS C MEYER D SCHEFFLER S SCHRAML B SCHUSTER RDRL WMM R DOWDING J ZABINSKI
1	NATIONAL INST OF STANDARDS & TECHLGY BLDG & FIRE RSRCH LAB J MAIN 100 BUREAU DR MS 8611 GAITHERSBURG MD 20899-8611	RDRL WMM A M MAHER J TZENG E WETZEL RDRL WMM B T BOGETTI B CHEESEMAN
3	DIR USARL RDRL D V WEISS RDRL SE J PELLEGRINO RDRL SES P A EDELSTEIN 2800 POWDER MILL RD ADELPHI MD 20783-1197	C FOUNTZOULAS D HOPKINS B POWERS C RANDOW M VANLANDINGHAM R WILDMAN C F YEN RDRL WMM D E CHIN K CHO R HOWELL RDRL WMM E
<u>ABERDEEN PROVING GROUND</u>		M COLE
103	DIR USARL RDRL WM B FORCH S KARNA J MCCAULEY P PLOSTINS J SMITH RDRL WML J NEWILL	T JESSEN J LASALVIA J SANDS RDRL WMM F L KECSKES S MATHAUDHU RDRL WML G J ANDZELM A RAWLETT

NO. OF  
COPIES ORGANIZATION

RDRL WMP  
P BAKER  
S SCHOENFELD  
RDRL WMP B  
R BECKER  
S BILYK  
D CASEM  
J CLAYTON  
M GREENFIELD  
C HOPPEL  
R KRAFT  
B LEAVY  
B LOVE  
M SCHEIDLER  
T WEERASOOPYIA  
C WILLIAMS (10 CPS)  
RDRL WMP C  
T BJERKE  
S SEGLETES  
G BOYCE  
R MUDD  
T DIGLIANI  
N BRUCHEY  
W WALTERS  
RDRL WMP D  
R DONEY  
J RUNYEON  
B SCOTT  
D KLEPONIS  
K STOFFEL  
RDRL WMP E  
M BURKINS  
W GOOCH  
T JONES  
M LOVE  
RDRL WMP F  
R BITTING  
M CHOWDHURY  
E FIORAVANTE  
A FRYDMAN  
N GNIAZDOWSKI  
R GUPTA  
RDRL WMP G  
N ELDREGE  
R EHLERS  
W BUKOWSKI  
B KRZEWINSKI  
S KUKUCK  
R BANTON  
D KOOKER  
G PEHRSON

INTENTIONALLY LEFT BLANK.